THE JOURNAL OF PHYSICAL CHEMISTRY C

Article

pubs.acs.org/JPCC

Hydrogen Bond Dynamics at Water/Pt Interfaces

Pablo E. Videla,[†] Lisandro Ansourian,[†] and Daniel Laria*[,†,‡]

[†]Departamento de Química Inorgánica, Analítica y Química-Física and INQUIMAE-CONICET, Facultad de Ciencias Exactas y Naturales, Universidad de Buenos Aires Ciudad Universitaria, Pabellón II, 1428 Buenos Aires, Argentina

[‡]Departamento de Física de la Materia Condensada, Comisión Nacional de Energía Atómica, Avenida Libertador 8250, 1429 Buenos Aires, Argentina

ABSTRACT: We present results from computer simulations that shed light on structural and dynamic characteristics of hydrogen bonding of aqueous phases at ambient conditions, at the close vicinity of electrified metal interfaces. Our simulation strategy relied on the consideration of a Hamiltonian that explicitly incorporates effects from polarization fluctuations at the metal surface, induced by the instantaneous local electric field promoted by the partial charges at the solvent molecules. Compared to bulk environments, our results reveal important modifications in the hydrogen bond architectures that critically depend on the atomic arrangements of the interfaces exposed to the liquid phases and the net charges allocated at the metal plates. These modifications have equally important consequences on the characteristic time scales describing the ruptures of hydrogen bonds which are operated by mechanisms which are absent in descriptions that omit atomic detail and polarization fluctuations at the metal plates. We also analyze how the latter modifications are translated into spectral shifts in the stretching bands of infrared spectra of water adlayers.

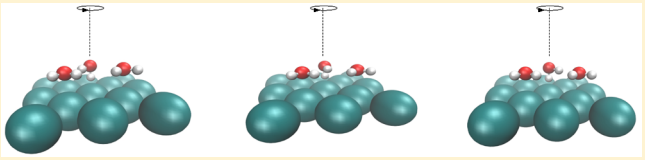

INTRODUCTION

Water/metal interfaces host the vast majority of reactive processes relevant to interfacial electrochemistry.[1] These phenomena include not only fundamental processes involving, for example, charge transfer,[2−7] but also a variety of reactions of technological relevance in areas such as energy production,[8] heterogeneous electrocatalysis,[9] corrosion,[10] and biotechnology.[11]

The usual routes to gain microscopic insights into the behavior of water at these interfaces rely on experimental signals and quantum calculations of systems at cryogenic temperatures.[12,13] The list of studies spans from the consideration of the simplest water−monomer adsorption case,[14,15] up to examinations of more complex, three-dimensional structures.[16,17] The picture that emerges from these analyses reveals the lack of a general treatment to account for the variety of planar network structures observed. As such, spatial and orientational correlations in the adsorbed layers would be the result of complex interplays between water−water and the particular water−metal interaction considered. These effects normally exhibit comparable magnitudes and competing characteristics.[13,18,19]

The consideration of macroscopic liquid phases in contact with metal surfaces introduces new relevant ingredients to this already complex description.[20−23] Most notably are those related to the appropriate treatment of the role played by thermal fluctuations. A recent series of simulation studies has demonstrated that water adlayers in contact with metal interfaces exhibit new collective behaviors, extending across mesoscopic spatial domains[24−26] and with characteristic time scales stretched well beyond those describing microscopic relaxations in normal liquid phases.[27−29] These modifications are not restricted to the closest water layer in contact with the metal, but it would also include alterations in the hydrogen bond (HB) architecture linking the latter with inner, bulklike regions, leading to local scenarios closer to the ones prevailing at the vicinity of large hydrophobic probes.[24]

The manifestation of these features spurred our interest in investigating the impact of the presence of a macroscopic planar metal surface on the HB dynamics at the closest adlayers. The latter dynamics modulates the kinetics of practically all reactive process in aqueous solutions. As a consequence, numerous studies have been conducted in the past to unveil the mechanisms that control the rupture and recompositions of intermolecular bonds in aqueous system. Without being exhaustive, the list includes bulk homogeneous phases,[30−34] water at extreme temperatures[35] and at metastable supercooled conditions,[36] water at solvation shells of simple electrolytes,[37,38] hydrophobic solutes,[39] and macromolecules[40−42] and interfacial environments, such as water in contact with silica walls,[43] water under confinement,[44,45] and water/air interfaces.[46−48]

In what follows, we will present molecular dynamics results that provide a microscopic perspective of the mechanisms that control HB dynamics at different water/Pt interfaces. Our model follows closely the one adopted in previous analysis.[24,25,49] As a key feature, the simulation procedure provides an adequate treatment of solvent induced local polarization fluctuations at the metal plates, satisfying basic electrostatic boundary conditions. This element, in turn, has important consequences modulating back the dynamics of the solvent

Received: July 26, 2016
Revised: October 5, 2016
Published: November 7, 2016

DOI: 10.1021/acs.jpcc.6b07504
J. Phys. Chem. C 2016, 120, 27276−27284

bonding, opening possibilities of different mechanistic descriptions of the ruptures and recompositions of HBs. As a complement, we also examine possibilities of assessing the extent of the local modifications in the strengths of different HB connectivities from spectral shifts operated in the stretching band of the infrared spectra of the adlayers.

The organization of the present paper is as follows: Section II includes a description of the model and the most important technical details of our simulation procedure. The main results of the work appear in Section III: We begin by presenting the basic elements that characterize the HB structure of water at Pt(100) and Pt(111) that will serve to rationalize the dynamical analysis that follows. The central part of Section III contains results of HB lifetimes and the descriptions of different mechanisms that drive HB ruptures. The analysis of the spectral characteristics of water adlayers closes the presentation of the simulation results. In Section IV, we summarize the most important conclusions of the work.

MODEL AND SIMULATION PROCEDURE

The systems under investigation were composed of N_w water molecules confined within two parallel Pt electrodes, fixed at $z = \pm 25$ Å. The systems were periodic, except along the z-axis which we made to coincide with the direction perpendicular to the plates. Each Pt electrode consisted of three atomic layers, with closest atomic separations set at 2.77 Å. The Pt atoms were arranged so that the interfaces exposed to the fluid phases were either of the Pt(100) type or of the Pt(111) type. For the former cases, the linear dimensions of the electrodes were 23.52 Å × 23.52 Å, whereas for the latter ones, the lengths were 22.16 Å × 24.0 Å. In all simulation runs, the number of water molecules—typically of the order of $N_w \sim 850-900$—was adjusted to bring the local solvent densities at midpoint locations with respect to the positions of the plates equal to the standard value at ambient conditions.

To model water−water interactions, we adopted a revised version[50] of the flexible SPC force field developed by Toukan and Rahman.[51] This modified version was specifically tailored to reproduce experimental features of the infrared spectral bands of water[52] at ambient conditions, without introducing sensible modifications in the rest of the predictions of the original version. Following previous studies,[24−27,29] water−Pt interactions were taken from ref 49 without further changes. Our simulation procedure included explicit polarization effects on the electrodes by considering that each Pt atom carries a fluctuating Gaussian charge (with width adjusted at 0.505 Å) that responds to the instantaneous local electric field generated by the rest of the charges in the electrodes and in the solvent sites.[49] As such, at each step of the simulation runs, all metal charges were adjusted, so as to satisfy the electrostatic boundary condition related to the constancy of a preset electrical potential, V_0, at the positions of all atoms within a particular electrode.

To treat the long-range nature of the Coulomb forces, we adopted the Ewald summation method complemented with a correction term, proposed by Yeh et al.[53,54] We tested that the latter scheme provides similar results to those obtained by implementing two-dimensional Ewald sums with slab geometries.[55,56] Equilibrium properties were computed from averages collected along ∼0.5 ns canonical runs, with temperature control operated via a Nosé Hoover thermostat.[57,58] Dynamical information was obtained from 10 statistically independent microcanonical runs, each one lasting typically 200 ps, whose initial conditions were taken from canonical trajectories after several heating treatments at temperatures of the order of ∼600 K. For each Pt−H_2O interface, three different values of $\Delta\Psi = 2V_0$ were considered, namely, 0, 2, and 5 V. For these voltages, the average charge densities at each one of the Pt(100) electrodes were found to be $\sigma_Q = 0.01$, 5.2, and 12.6 μC cm^{-2}, respectively. On the other hand, for Pt(111) electrodes, we registered slightly higher charge densities, namely, $\sigma_Q = 0.01$, 5.9, and 14.8 μC cm^{-2}. Typically, we found that ∼95% of the total charges at the electrodes were localized at the innermost layers, in contact with the liquid phases. In all cases, differences between the average values of the total charges at the two plates were less than 1%.

RESULTS

Structural Characteristics of HB. Before analyzing the dynamical characteristics of HB at the vicinity of the Pt electrodes, it will be instructive to present a brief overview of the local structural features of the intermolecular bonding at these environments. The results presented here for the flexible SPC model complement previous ones reported for the rigid SPC/E force field.[24,25]

Our starting point will be the examination of solvent density fields of the type

$$\rho_\alpha(z) = \frac{1}{A\rho_\alpha^{blk}} \sum_{i=1}^{N_w} \langle \delta(z_i^\alpha - z) \rangle \quad (1)$$

where z_i^α represents the z-coordinate of the ith atom of species α (α = O, H) and ρ_α^{blk} denotes the corresponding bulk densities. In Figure 1 we present results for O-plots at different values of

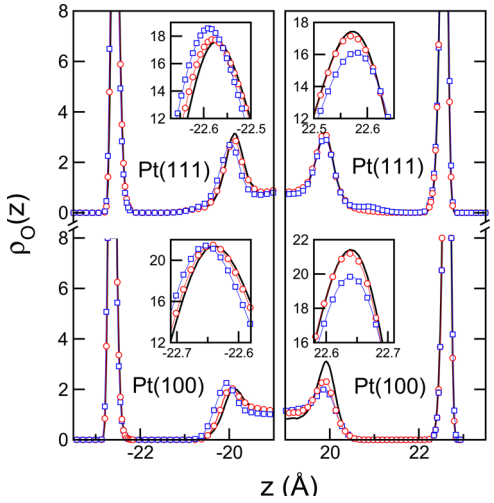

Figure 1. Local density fluctuations for oxygen water atoms in the close vicinity of Pt electrodes for $\Delta\Psi = 0$ V (solid line), 2 V (red circles), and 5 V (blue squares). The anode (cathode) is located at $z = -25$ Å (+25 Å).

$\Delta\Psi$. As a distinctive feature one observes the presence of main peaks located 2.4 Å inward with respect to the position of the external electrodes, followed by ∼2 Å wide gaps, deprived from water, deeper into the bulk. The magnitudes of the main peaks—in all cases close to 20—reveal tightly adsorbed aqueous layers in contact with the metal.[24] Water packing looks slightly more marked at both Pt(100) interfaces, compared to the one observed next to Pt(111). A simple

DOI: 10.1021/acs.jpcc.6b07504
J. Phys. Chem. C 2016, 120, 27276−27284

calculation shows that the global surface density of water molecules is ∼0.13 Å^{-2} for the former case and ∼0.116 Å^{-2} for the latter one. The former value practically coincides with the surface density of metal atoms at the (100) face, confirming the marked propensity of the adsorbed water molecules to lie on top of each exposed atom in the metal substrate.

The interplay between the geometrical characteristics of the atomic arrangement in the underlying Pt substrates and the directionality in the intermolecular connectivity in water leads to well differentiated, two-dimensional spatial domains across the adsorbed layers that differ in their hydrogen bond patterns and dipolar correlations.[24,27] In particular, the adsorbed layer on Pt(100) is characterized by mesoscopic patches of water molecules exhibiting double-donor−double-acceptor characteristics, with typical sizes of the order of the nanometer. The boundaries between these domains correspond to "defect lines", along which orientational correlations present sharp modifications. Contrasting, the sixfold coordination prevailing in Pt(111) surfaces promotes structures with intermolecular connectivities characterized by mostly double-donor−single-acceptor motifs. As a result, their overall structures can be cast in terms of hexagonal rings enclosing vacant central sites, separated by more open, irregular structures, with lack of any evident short-range orientational order. Interestingly, in both cases, the presence of this variety of spatial domains introduces heterogeneous characteristics into the orientational dynamics of the adsorbed layers, with time scales spanning from the picosecond time domain—characteristic of small amplitude librations—up to a few tens of nanoseconds, which describe global reorganizations involving high and low orientational mobility domains.[27]

Although the presence of the external electric fields does not modify the magnitudes and positions of the peaks of $\rho_O(z)$ in a sensible fashion (see insets), the analysis of the plots for $\rho_H(z)$, which are shown in Figure 2, reveals clear field-induced

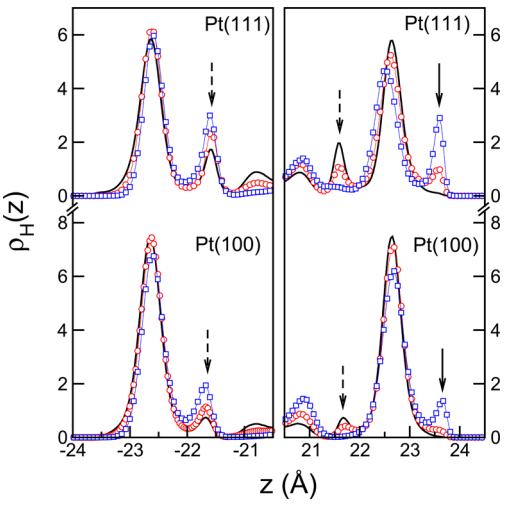

Figure 2. Same as Figure 1 for H-sites.

modifications. Starting with ΔΨ = 0 V scenarios, the plots for $\rho_H(z)$ present main peaks whose positions coincide with those previously observed for $\rho_O(z)$, corroborating the presence of a planar hydrogen bonded network spanning across the electrode surfaces. In addition, one can also observe secondary peaks at ∼± 21.7 Å (indicated by dashed arrows), revealing hydrogen bonding between the adsorbed water molecules and neighboring ones in the adjacent "bulk" region. The fraction of these out-of-plane bonds compared to the in-plane ones is small—of the order of ∼5−10%—a fact that corroborates the hydrophobic characteristics of the tightly adsorbed layers reported previously. The response to external electric fields at the anodes leads to mild increments in the hydrogen bonding between the adsorbed and the closest water molecules in the "bulk". A similar analysis performed near the cathodes reveals the following: (i) first, a gradual decrease of the original secondary peaks, which practically disappears for ΔΨ = 5 V; (ii) second, a similar gradual reduction of the population of in-plane hydrogen atoms, and (iii) the presence of new peaks at $z \sim$ +23.7 Å (indicated by solid arrows). Note that the magnitudes of the polarization responses of the adsorbed layers, expressed in terms of the modifications operated in the peak magnitudes, look somewhat more marked for the "less rigid" Pt(111) interfaces.

In order to unveil the characteristics of these modifications upon the original local architecture of hydrogen bonding, it will be instructive to pause for a moment to re-examine the gross features describing solvent induced polarization fluctuations at the Pt atoms. Following previous analysis,[25,26] we concentrated in examining the atomic charge distributions in the metal, namely

$$p_e(q) = \frac{1}{N_{Pt}} \sum_{i=1}^{N_{Pt}} \langle \delta(q - q_i) \rangle \quad (2)$$

where q_i represents the partial charge at the ith Pt atom and N_{Pt} represents the number of Pt atoms in contact with the aqueous phase. Results for $p_e(q)$ are shown in Figure 3. The plots for the

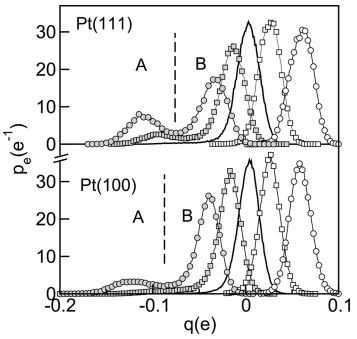

Figure 3. Probability distribution for atomic charges at the innermost surfaces of the Pt electrodes at different voltages: 0 V (solid line); 2 V (squares); 5 V (circles). Positively charged wall (white symbols); negatively charged wall (gray symbols). The vertical dashed lines determine boundaries for Pt$^{\mathcal{A}}$ and Pt$^{\mathcal{B}}$ atoms for ΔΨ = 5 V (see text).

anodes contrast sharply with the ones for the negative plates. The former ones are reasonably well described by Gaussian profiles whereas, for negatively charged plates, the distributions exhibit clear bimodal characters. As expected, this bimodality in the charge distribution looks more enhanced the higher the applied voltages and seems to be more marked at Pt(111) surfaces.

To facilitate our description, in what follows, we will establish two categories, $\mathcal{A}$ and $\mathcal{B}$, to discriminate Pt atoms with high and low polarizations, respectively. The boundaries between these two categories were set at the local minima of the corresponding distributions. For the particular case of ΔΨ = 5 V, approximately ∼10% of the Pt sites were found to be of type

DOI: 10.1021/acs.jpcc.6b07504
J. Phys. Chem. C 2016, 120, 27276−27284

$\mathcal{A}$ at Pt(100) interfaces whereas, for Pt(111) interfaces, that percentage was found to be close to ∼30%. Yet, we remark that the average values of the charge at $Pt^{\mathcal{A}}$ sites in Pt(100) interfaces are slightly more negative that the corresponding values for the Pt(111) interface.

With this classification in mind, we proceed by computing site−site solvent−metal spatial correlations of the type

$$\rho_{Pt^k\alpha}(r) = \frac{1}{4\pi r^2 N_{Pt}^k} \sum_{i=1}^{N_{Pt^k}} \sum_{j=1}^{N_w} \langle \delta(r - |\mathbf{r}_\alpha^j - \mathbf{r}_{Pt^k}^i|) \rangle \quad (3)$$

where $\mathbf{r}_{Pt^k}^i$ denotes the position of the ith Pt atom (i = 1, ..., N_{Pt^k}) of type k ($k = \mathcal{A}, \mathcal{B}$). As an illustrative example, we will examine the density profiles shown in Figure 4 which

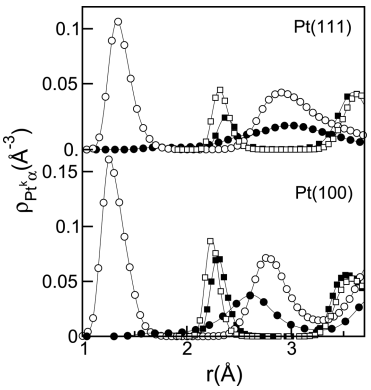

Figure 4. Site−site Pt−W correlation functions for ΔΨ = 5 V. $Pt^{\mathcal{A}}$-O_W: open squares; $Pt^{\mathcal{A}}$-H_W: open circles; $Pt^{\mathcal{B}}$-O_W: black squares; $Pt^{\mathcal{B}}$-H_W: black circles.

correspond to cathodes, for ΔΨ = 5 V. The characteristics of $\rho_{Pt^k\alpha}(r)$ for $k = \mathcal{A}$ and $k = \mathcal{B}$ contrast sharply. In the former case, the main peaks correspond to $Pt^{\mathcal{A}}$−H correlations (open circles); they are located at r = 1.26 Å and r = 1.34 Å, and their cumulative integrals add up to 0.93 and 0.7 for Pt(100) and Pt(111) interfaces, respectively. Similar populations are registered under the first peaks of $\rho_{Pt^{\mathcal{A}}O}$ (open squares) located at r = 2.24 Å and r = 2.31 Å, revealing practically colinear O−H···$Pt^{\mathcal{A}}$ connectivities. In addition, the much broader, secondary peaks of $\rho_{Pt^{\mathcal{A}}H}$ at $r \sim 2.80$ Å correspond to H-sites that participate in the original in-plane connectivity that would prevail even in the absence of net charge at the electrodes. The analysis of the water density next to $Pt^{\mathcal{B}}$ atoms (black symbols) shows absence of the previous water−Pt hydrogen bonding; the closest peaks now correspond to still on-top, oxygen sites and look slightly shifted, deeper into the bulk. The corresponding H-peaks located at $r \sim 2.75$ Å integrate twice the values one would obtain for the O-sites and correspond to H-sites lying at in-plane locations.

Armed with this set of results, the overall picture that emerges for the hydrogen bonding at the vicinity of charged Pt surfaces can be summarized as follows: In all cases, polarization effects leads to a decrease in the extent of in-plane H-bonding. At positively charged electrodes, this modification is compensated with an increment in the perpendicular bonding involving the adsorbed layer and the closest water shell in the bulk. At the cathodes, the gradual modifications lead to a disappearance of the minor connectivity with the bulk, along with the gradual manifestation of two different types of intermolecular connectivities: on the one hand, the persistence of the original in-plane H-bond connecting double-donor−double-acceptor molecules, lying on top of $Pt^{\mathcal{B}}$ sites in the substrate and, on the other, a new class of O−H··· $Pt^{\mathcal{A}}$ bonding, localized on top of the much more polarized $Pt^{\mathcal{A}}$ sites. The fraction of molecules participating in this new perpendicular connectivity was found to be smaller at Pt(100) interfaces. However, based on the local characteristics of water−substrate spatial correlations, in the latter cases, H-bonding looks somewhat stronger compared to what is observed at Pt(111) interfaces. As we will show in the next section, these modifications will have important implications in the dynamical aspects of HB breaking and reconstruction.

Hydrogen Bond Dynamics. Our dynamical analysis will be focused on determining τ_{HB}, the average lifetime of a tagged HB connecting a pair of water molecules lying at the adsorbed layers. The usual procedure to estimate τ_{HB} relies on the analysis of equilibrium time correlation functions of the following form:

$$C_{HB} = \frac{\langle \delta h_{ij}(0) \delta h_{ij}(t) \rangle}{\langle (\delta h_{ij})^2 \rangle} \quad (4)$$

Different definitions have been adopted in previous studies for the characteristic function $h_{ij}(t)$.[32] In the present case, we adopted the criterion which establishes that $h_{ij}(t)$ is one if a tagged (i,j) pair of water molecules remains hydrogen bonded continuously during the time interval $[0, t]$ and zero otherwise. The identification of the different hydrogen bonds was performed according to the geometrical criterion established in previous studies.[30−32]

Results for $C_{HB}(t)$ for ΔΨ = 0 V and ΔΨ = 5 V and the corresponding estimates for τ_{HB} are displayed in Figure 5. The latter values were computed from time integrals of the simulated $C_{HB}(t)$, assuming mono- and biexponential decays for Pt(100) and Pt(111) interfaces, respectively, beyond 10 ps. HB lifetimes at Pt(111) interfaces are practically twice as long

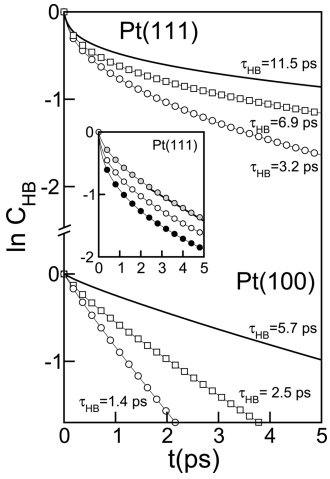

Figure 5. Hydrogen bond population relaxation at different water−Pt interfaces and applied voltages. ΔΨ = 0 V: solid lines; ΔΨ = 5 V, positive plate: open squares; ΔΨ = 5 V, negative plate: open circles. The inset shows the decomposition of C_{HB} into in-plane (black circles) and out-of-plane (gray circles) mechanisms (ΔΨ = 5 V, negative plate). The thick solid line corresponds to a linear fit for t > 2 ps.

DOI: 10.1021/acs.jpcc.6b07504
J. Phys. Chem. C 2016, 120, 27276−27284

as the values obtained at Pt(100) electrodes and, in all cases, become shorter for charged electrodes. In all cases the values of τ_{HB} are larger than those reported in simulations for bulk water at ambient conditions which are, typically, in the ∼0.5−1 ps time domain.[32] More interestingly, the two sets of curves shown at the top and bottom parts of the figure differ at a qualitative level. For Pt(100) interfaces, all decays exhibit single-exponential characteristics which suggest that HB breaking episodes, in principle, could be cast in terms of uncorrelated events obeying Poisson statistics.

The direct inspection of a large number of trajectories revealed details of two main mechanisms that contribute to the overall decay of the HB population. The initial stage involves the breakage of one HB (indicated as $OH_1\cdots O_{a1}$ in Figure 6) in

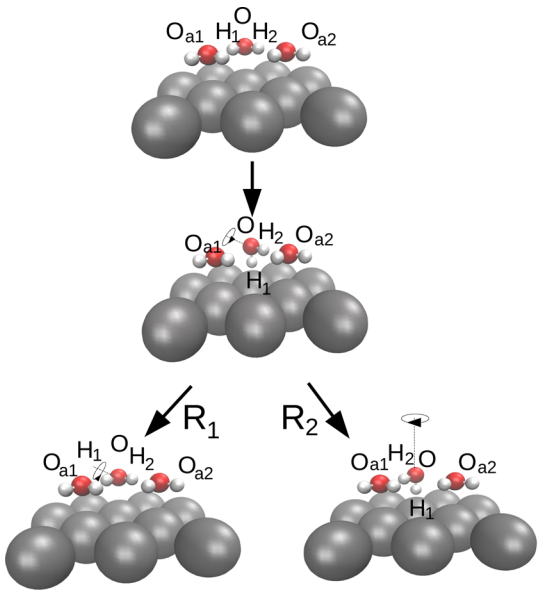

Figure 6. Proposed mechanisms for HB ruptures for water adsorbed at Pt(100) cathodes. Out-of-plane rotation: route $\mathcal{R}_1$; in-plane-rotation: route $\mathcal{R}_2$ (see text).

a tagged double-donor molecule. This loss of intermolecular connectivity is normally operated via a rotation along the $OH_2\cdots O_{a2}$ axis, leading to a new HB which, for the particular case of a negatively charged interface, is established with an underlying Pt atom as acceptor. Following this initial flipping motion, and within a brief, subpicosecond time interval, two alternative process may occur: (i) in approximately 70% of the cases, the broken $OH_1\cdots O_{a1}$ is quickly reestablished, (route $\mathcal{R}_1$ in Figure 6); (ii) in the rest of the episodes, the initial flip triggers the rupture of the second, originally intact, $OH_2\cdots O_{a2}$ bond, via a ∼ 90°, in-plane rotation, leading to the subsequent formation of a new $O{-}H_2\cdots O_{a1}$ bond (route $\mathcal{R}_2$ in Figure 6).

The fact that the values τ_{HB} are smaller at charged electrodes compared to the $\Delta\Psi$ = 0 V case would indicate a weakening in the original in-plane HB network, benefiting more frequent O−H transitions from parallel to perpendicular orientations with respect to the metal substrate. Incidentally, we remark that, at the anode, such reorientations would also require the energetically unfavorable approach of a new acceptor water molecule from the bulk into the local hydrophobic environment next to the adsorbed layer. This would explain the slower rate observed at the positively charged interface compared to one registered at the opposite plate, where the new acceptor partners correspond to a close neighbor, highly polarized, $Pt^{\mathcal{A}}$ sites.

The decays of $C_{HB}(t)$ for Pt(111) surfaces shown in Figure 5 not only reveal longer characteristic times compared to Pt(100) results but, more importantly, exhibit clear nonexponential behaviors, suggesting the presence of more complex relaxation mechanisms. In order to shed light on the causes of these peculiarities, we found it instructive to analyze separately the characteristics of the trajectories involving the two HB breaking routes previously described. To do so, we split the full $C_{HB}(t)$ into a weighted sum of two contributions, namely

$$C_{HB}(t) = x_{ip}C^{ip}_{HB}(t) + x_{op}C^{op}_{HB}(t) \quad (5)$$

where $C^{i}_{HB}(t)$ (i = ip, op) corresponds to normalized time correlation functions computed from trajectories in which the mechanism of the rupture of the tagged HB is operated via either an out-of-plane or an in-plane rotation, respectively and x_i corresponds to the fraction of the total trajectories of each type. Results of $C_{HB}(t)$ and its decomposition into C^{ip}_{HB} and C^{op}_{HB} for the $\Delta\Psi$ = 5 V case are shown in the inset of the Figure 5. One observes that, contrasting with the decay of C^{op}_{HB} which looks single-exponential after ∼2 ps (gray circles), the decay of C^{ip}_{HB} exhibits nonexponential relaxation along the ∼5 ps time interval (see curve with black circles). Moreover, at these interfaces, we found that the fraction of trajectories exhibiting in-plane HB ruptures was x_{ip} ∼ 0.6, indicating that, as a result of the more open structures of the adsorbed layers, HB exchanges involving in-plane rotations should not be necessarily preceded by out-plane rotation episodes, as we found in Pt(100) interfaces.

At this time, it will be useful to briefly digress on the characteristics of the extended jump model mechanism proposed by Laage and Hynes[59,60] to describe HB dynamics in condensed phases. Instead of describing the mechanism of exchange of HB acceptors in terms of small amplitude rotations with diffusive characteristics, the latter model postulates that the key elements controlling the passages over transition states involve an interplay between antisymmetric translational motions coupled to large amplitude jumps which, in conventional condensed phases, are of the order of ∼70°. In the presence context, the consideration of the first translational ingredient should be less important, given the strong interactions between the adsorbed layer and the substrate that pin acceptor and donor water molecules at top positions of neighboring Pt atoms. More relevant should be the examination of the variety of orientational modifications involved in in-plane H-bond exchanges. A simple geometrical analysis shows that rotational exchanges involving molecules participating in hexagonal ring structures require angular motions with amplitudes close to ∼120°. Contrasting, in-plane exchanges localized in the rest of much more disordered domains require much smaller, i.e., ∼ 60°, overall amplitudes. As such, this diversity of rotational amplitudes should be reflected in an equal variety of free energy barriers and characteristic time scales, giving support to the absence of single-exponential decays found in C^{ip}_{HB}.

Infrared Spectra. The second dynamical aspect that we investigated concerns the possibility of detecting voltage-induced changes in the characteristics of hydrogen bond connectivity at water/Pt interfaces from the analysis of spectral shifts in infrared spectra. At present, several surface sensitive spectroscopic techniques provide direct experimental informa-

DOI: 10.1021/acs.jpcc.6b07504
J. Phys. Chem. C 2016, 120, 27276−27284

tion about spectral shifts for aqueous adlayers in contact with metallic surfaces in solution.

In particular, in what follows, we will focus attention on the modifications operated at cathodic surfaces, where the magnitude of the changes in the HB architecture are likely to be more marked. In Figure 7 we present results for the

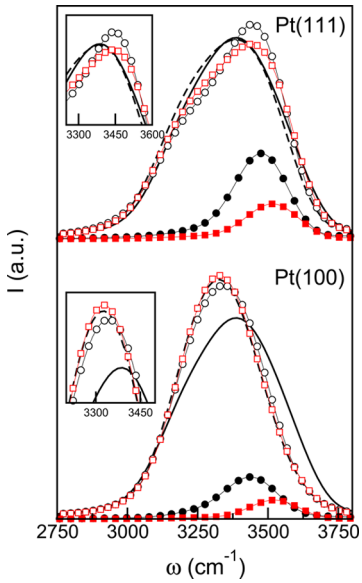

Figure 7. Stretching bands of infrared spectra for water adsorbed at W−Pt interfaces at different voltages. $\Delta\Psi$ = 0 V: dashed lines; $\Delta\Psi$ = 2 V, negatively charged wall: open red squares; $\Delta\Psi$ = 5 V, negatively charged wall: open black circles. The curves with solid symbols correspond to H atoms participating in O−H···Pt$^{\mathcal{A}}$ bonds (see text) at voltages similar to the corresponding open-symbol curves. Also shown are results for bulk water: solid lines.

stretching band of the infrared spectrum of water at the two water−Pt interfaces investigated. In order to facilitate the comparisons that will follow, all spectra in the figure present equal areas, except those indicated by filled symbols. Within our classical treatment, the line shapes were approximated from Fourier transforms of time correlation functions of the velocities of the H atoms,[61] namely

$$I(\omega) = \int_{-\infty}^{\infty} C_{vv}(t)\cos \omega t \, dt \tag{6}$$

where

$$C_{vv}(t) \propto \sum_{i=1} \langle \mathbf{v}_i^{H}(t)\mathbf{v}_i^{H}(0)\rangle \tag{7}$$

The large disparity between the characteristic relaxation times of $C_{vv}(t)$ (usually below ∼1 ps) and the mean residence times of water molecules at the ad-layers (at least, 3 orders of magnitude larger)[28] allowed us to restrict the sampling in eq 7 to adsorbed molecules exclusively. As a reference, in Figure 7, we have also included results for bulk water at ambient conditions computed with the flexible SPC model. The latter spectrum presents a broad asymmetric band centered at ω_{blk} = 3380 cm^{-1}, very close to the experimental value.[52]

Compared to bulk signals, the simulated line shapes for $\Delta\Psi$ = 0 V (dashed lines) show distinctive characteristics depending on the particular Pt interface considered. For the Pt(100) case, the main modification involves a $\Delta\omega \sim -60$ cm^{-1} red shift. Contrasting, the signal from the adsorbed water molecules at the Pt(111) surface practically coincides with the bulk values (see insets). The shift in the Pt(100) signal, in turn, would indicate the stronger character of H-bonds across the highly regular, in-plane network articulated via double-donor−double-acceptor molecules, in contraposition with bulk scenarios. Moreover, the variety of intermolecular connectivities observed throughout the much more open, intermolecular network at the water−Pt(111) interface would yield global results that do not differ substantially from what is obtained in three-dimensional bulk environments.

The incorporation of net charge at the electrodes leads to (i) more marked asymmetries between the low- and high-frequency flanks of the stretching bands and (ii) overall blue shifts with respect to the $\Delta\Psi$ = 0 V results, most notably in the more susceptible water−Pt(111) interface. To look into the origin of the latter modifications, we found it useful to decompose the total correlation function $C_{vv}(t)$ into separate contributions from H-atoms participating in in-plane and in out-of-plane H-bonds. Results from the latter category appear in Figure 7 with filled symbols. One can observe the following: (i) at both interfaces, contributions from out-of-plane H-bonds lie at the high-frequency shoulder of the bands revealing their weaker nature, compared to in-plane ones; (ii) as expected, these bonds become weaker, the smaller the magnitude of the charge allocated at the underlying Pt$^{\mathcal{A}}$ sites; (iii) their global contributions to the overall line shapes—evaluated in terms of the magnitudes of the peaks—is larger for Pt(111) surfaces, a fact that goes hand in hand with the larger fraction of Pt$^{\mathcal{A}}$ atoms with respect to Pt$^{\mathcal{B}}$ ones, at these interfaces (see Figure 3); (iv) voltage induced blue shifts at the Pt(100) cathodes look somewhat milder than the ones registered at the Pt(111) surfaces, an observation that also agrees with the stronger character of the OH···Pt$^{\mathcal{A}}$ bonds observed at the former surfaces which is also clearly perceived by comparing the plots for $\rho_{Pt^{\mathcal{A}}H}(r)$, shown in Figure 4.

Direct experimental support to the previous observations is not straightforward because, in most cases, the information is obtained from electrolyte solutions, in which the presence of different adsorbed ionic species are likely to modify water signals.[62] Moreover, the results obtained from different techniques are, in some cases, inconclusive. For example, reflectance spectra from $HClO_4$ aqueous solutions in contact with Pt(111) interfaces exhibit red shifts in the vibrational band of water, as the potential of the plate gets more negative.[63] On the other hand, more recent results from infrared reflection absorption spectroscopy (IRAS) experiments combined with attenuated-total-reflection techniques performed on polycrystalline Pt electrodes would suggest opposite trends; i.e., blue shifts are observed as the wall potential moves down, below the potential-of-zero-charge value.[64,65] In addition, similar trends have also been reported for aqueous solutions of perchloric acid[66] and sulfuric acid[67] in contact with Au(111) electrodes. Interestingly, Hirota et al.[68] have reported IRAS results for $HClO_4$ and HF solutions in contact with Pt(111) showing the appearance of a new signal at higher frequencies of the order of ∼3700 cm^{-1}, as the potential of the electrode gets more negative. This feature was ascribed to the presence of "nonbonded" water monomers. As such, and within the present context, it seems reasonable to speculate on possible connections between the presence of these "free" monomers

DOI: 10.1021/acs.jpcc.6b07504
J. Phys. Chem. C 2016, 120, 27276−27284

and water molecules participating in the much weaker OH···$Pt^{\mathcal{A}}$ bonds shown in the present simulations.

CONCLUDING REMARKS

The computer simulation results presented in this work provide new insights into the modifications operated in the dynamics of the intermolecular connectivity of the solvent at the vicinity of different water−Pt interfaces. Special attention was focused on gauging the impacts of two controlling agents on the latter dynamics: (i) the particular atomic spatial arrangement at the exposed interface, determining the local characteristics of Pt−water and water−water connectivity, and (ii) the electrical charges allocated at the solid phases, polarizing the adjacent water layers. As a general conclusion, our simulations reveal that the characteristic time scales describing the ruptures of water−water hydrogen bonds at these interfaces are normally longer, compared to those observed in the bulk; moreover, these differences become more marked as the average electrical coupling between the solvent and the metal electrode decreases.

In addition, two different reactive mechanisms were identified. At water−Pt(100) interfaces, HB exchanges requires initial stages in which the double-donor−double-acceptor connectivity that spans across the planar interface is disrupted by out-of-plane rotations. At negatively charged interfaces, these episodes mostly involve the formation of new bonds with underlying $Pt^{\mathcal{A}}$ atoms and become gradually less frequent, the smaller the polarization effects on the solvent induced by the local charges allocated at the electrodes. For the limiting, $V_0 = 0$, case, the prevailing flip directions reverse and new bonds are established with water molecules approaching the adsorbed adlayer from deeper regions in the bulk phase. In all cases, and within subpicosend time intervals, these initial out-of-plane rotations open possibilities for a second channel of rupture involving in-plane, 90° rotations, in which the water molecules pivot around the OH bond perpendicular to the Pt surface.

The somewhat more open structure of the hydrogen bonded network that prevails at Pt(111) interfaces makes water intermolecular connectivity more "resistant" to modifications. As such, and compared to Pt(100) scenarios, all characteristic time scales stretch by a factor of ∼2. In addition, HB population relaxations not only exhibit slower decays but also a wider variety of characteristic time scales. This feature is clearly detectable in trajectories in which the HB ruptures involve in-plane-rotations, where angular motions may exhibit well differentiated amplitudes, depending on whether the tagged donor−acceptor pairs involve atoms in hexagonal rings or those lying in regions with less marked orientational order.

We feel important to remark that the interplay established between, on the one hand, solvent polarization fluctuations controlling the magnitudes charges at the Pt atoms and, on the other, the latter charges modulating back HB ruptures in the solvent, represents a key ingredient in the present description which would be absent in simulation strategies relying on the consideration of continuum models[46] or uniformly distributed charges across electrodes.[23] In this respect, one could anticipate that dynamical predictions otherwise obtained using the latter alternative would differ from the present ones in a sensible fashion. Still, a consistent treatment of polarization fluctuations should include additional contributions from solvent species. Note that, in the present case, such fluctuations are only partially considered by the incorporation of flexibility in the internal degrees of freedom. In this respect, and taking into account simulation results from polarizable and nonpolarizable rigid models reported by Xu et al.,[69] our predictions for τ_{HB} are likely to be understimated.

We finally analyzed how the latter modifications are translated into spectral shifts in the stretching bands of infrared spectra restricted to water molecules lying at cathodic adlayers. Compared with the bulk line shape, the stretching bands for water at Pt(100) present red shifts, demonstrating the stronger nature of hydrogen bonds across the 2*D* network, compared to the conventional 3*D* bulk structure; much milder blue shifts are also observed as the charge at the electrode increases. In all cases, signals from OH stretchings participating in O−H···$Pt^{\mathcal{A}}$ bonds lie at the high-frequency shoulders of stretching bands signalizing their weaker nature compared to the ones prevailing across the corresponding adlayers. In this respect, the scenario here resembles the one observed at the vicinity of hydrophobic surfaces where an equivalent correspondence between dangling OH bonds and spectral blue shifts have been established in previous experimental[70,71] and simulation[43] studies.

Before closing this paper we would like to briefly comment on the limitations of the model presented here, more specifically, on those inherent to the approximate treatment of interparticle interactions. Concerning the solvent, the recent advent of highly sophisticated potential energy functions based on hierarchical treatments of many-body effects has opened possibilities for highly accurate results for many structural and dynamical properties of aqueous phases, spanning from nanoclusters[72,73] up to bulk environments.[74−76] In particular, ref 77 contains a comparative analysis in which the quality of the different treatments—starting from pairwise analytical energy functions as the one implemented here, up to many-body potential energy functions with different degrees of sophistication—are critically examined. Equally important to keep in mind are the limitations in our description of water−Pt interactions. For example, our approach disregards effects derived from dissociative processes in water[78] or charge transfer processes at the interfaces[79] that might modify in part our results and that could be explicitely incorporated at the expense of significant computational costs. Substrate-induced modifications in the electronic structure of the adsorbed solvent molecules are known to also modify the strength of water−water interactions in complex fashions, a fact that should also be reflected in modifications on the mechanisms of HB ruptures. As such, more elaborate descriptions of the overall solvent−solvent and solvent−metal potential energy surface should be performed in a consistent fashion which clearly represents a highly challenging implementation worth pursuing.

Still, and based on the quality of the present results along with those reported in previous studies employing treatments similar to the ones adopted here, we believe that our simulations still capture essential elements controlling the dynamics of hydrogen bonding at water−Pt interfaces, bringing physical support to their predictions and making them appropriate benchmarks for further improvements as the ones previously described.

AUTHOR INFORMATION

Corresponding Author

*E-mail: dhlaria@cnea.gov.ar. Phone: +54 (11)67727048. Fax: +54 (11)67727121.

DOI: 10.1021/acs.jpcc.6b07504
J. Phys. Chem. C 2016, 120, 27276−27284

Notes

The authors declare no competing financial interest.

■ ACKNOWLEDGMENTS

D.L. is a staff member of CONICET-ARGENTINA and acknowledges the support of this research from CONICET-Argentina (PIP 112-20110100464).

■ REFERENCES

(1) *Interfacial Electrochemistry: Theory, Experiments and Applications*; Wieckowski, A., Ed.; Marcel Dekker, Inc.: New York, 1999.
(2) Levich, V. G. *Kinetics of Reactions with Charge Transfer*. In *Physical Chemistry, An Advanced Treatise*; Eyring, H., Henderson, D., Jost, W., Eds.; Academic Press: New York, 1970.
(3) Kuznetsov, A. M. *Charge Transfer in Physics, Chemistry and Biology*; Gordon and Breach, Reading, PA, 1995.
(4) Miller, A. D.; Bezel, I.; Gaffney, K. J.; Garrett-Roel, S.; Liu, S. H.; Szymanski, P.; Harris, C. B. Electron Solvation in Two Dimensions. *Science* **2002**, *297*, 1163−1166.
(5) Stähler, J.; Bovensiepen, W.; Meyer, M.; Wolf, M. A Surface Science Approach to Ultrafast Electron Transfer and Solvation Dynamics at Interfaces. *Chem. Soc. Rev.* **2008**, *37*, 2180−2190.
(6) Wilhelm, F.; Schmickler, W.; Spohr, E. Proton Transfer to Charged Platinum Electrodes. *J. Phys.: Condens. Matter* **2010**, *22*, 175001.
(7) Cao, Z.; Kumar, R.; Peng, Y.; Voth, G. A. Proton Transport under External Applied Voltage. *J. Phys. Chem. B* **2014**, *118*, 8090−8098.
(8) Khaselev, O.; Tuner, J. A. A Monolithic Photovoltaic-Photoelectrochemical Device for Hydrogen Production via Water Splitting. *Science* **1998**, *280*, 425−427.
(9) Santos, E.; Quaino, P.; Schmickler, W. Theory of Electrocatalysis: Hydrogen Evolution and More. *Phys. Chem. Chem. Phys.* **2012**, *14*, 11224−11233.
(10) Roberge, P. R. *Handbook of Corrosion Engineering*; McGraw-Hill: New York, 2012.
(11) See, for example, *Applications of Electrochemistry and Nanotechnology in Biology and Medicine II*; Eliaz, N., Ed.; Springer: New York, 2012.
(12) Hodgson, A.; Haq, S. Water Adsorption and the Wetting of Metal Surfaces. *Surf. Sci. Rep.* **2009**, *64*, 381−451.
(13) Carrasco, J.; Hodgson, A.; Michaelides, A. A Molecular Perspective of Water at Metal Interfaces. *Nat. Mater.* **2012**, *11*, 667−674.
(14) Michaelides, A. Density Functional Theory Simulations of Water−Metal Interfaces: Waltzing Waters, A Novel 2D Ice Phase, and More. *Appl. Phys. A: Mater. Sci. Process.* **2006**, *85*, 415−425.
(15) Okuyama, H.; Hamada, I. Hydrogen-Bond Imaging and Engineering with a Scanning Tunnelling Microscope. *J. Phys. D: Appl. Phys.* **2011**, *44*, 464004.
(16) Kimmel, G. A.; Petrik, N. G.; Dohnálek, Z.; Kay, B. D. Crystalline Ice Growth on Pt(111): Observation of a Hydrophobic Water Monolayer. *Phys. Rev. Lett.* **2005**, *95*, 166102.
(17) Thürmer, K.; Bartelt, N. Growth of Multilayer Ice Films and the Formation of Cubic Ice Imaged with STM. *Phys. Rev. B: Condens. Matter Mater. Phys.* **2008**, *77*, 195425.
(18) Tatarkhanov, M.; Ogletree, D. F.; Rose, F.; Mitsui, T.; Fomin, E.; Maier, S.; Rose, M.; Cerda, J. I.; Salmeron, M. Metal- and Hydrogen-Bonding Competition during Water Adsorption on Pd(111) and Ru(0001). *J. Am. Chem. Soc.* **2009**, *131*, 18425−18434.
(19) Björneholm, O.; Hansen, M. H.; Hodgson, A.; Liu, L.-M.; Limmer, D. T.; Michaelides, A.; Pedevilla, P.; Rossmeisl, J.; Shen, H.; Tocci, G.; Tyrode, E.; Walz, M.; Werner, J.; Bluhm, H.; et al. Water at Interfaces. *Chem. Rev.* **2016**, *116*, 7698−7726.
(20) Spohr, E.; Heinzinger, K. Molecular Dynamics Study on the Water/Metal Interfacial Potential. *Ber. Bunsen-Ges. Phys. Chem.* **1998**, *92*, 1358−1363.
(21) Spohr, E. Computer Simulation of the Water/Platinum Interface. *J. Phys. Chem.* **1989**, *93*, 6171−6180.
(22) Raghavan, K.; Foster, K.; Berkowitz, M. Comparison of the Structure and Dynamics of Water at the Pt(111) and Pt(100) Interfaces: Molecular Dynamics Study. *Chem. Phys. Lett.* **1991**, *177*, 426−432.
(23) Xia, X.; Perera, L.; Essmann, U.; Berkowitz, M. L. The Structure of Water at Platinum/Water Interfaces. Molecular Dynamics Computer Simulations. *Surf. Sci.* **1995**, *335*, 401−415.
(24) Limmer, D. T.; Willard, A. P.; Madden, P.; Chandler, D. Hydration of Metal Surfaces Can Be Dynamically Heterogeneous and Hydrophobic. *Proc. Natl. Acad. Sci. U. S. A.* **2013**, *110*, 4200−4205.
(25) Willard, A. P.; Reed, S. K.; Madden, P. A.; Chandler, D. C. Water at an Electrochemical Interface—A Simulation Study. *Faraday Discuss.* **2009**, *141*, 423−441.
(26) Limmer, D. T.; Merlet, C.; Salanne, M.; Chandler, D.; Madden, P. A.; van Roij, R.; Rotenberg, B. Charge Fluctuations in Nanoscale Capacitors. *Phys. Rev. Lett.* **2013**, *111*, 106102.
(27) Willard, A. P.; Limmer, D. T.; Madden, P. A.; Chandler, D. Characterizing Heterogeneous Dynamics at Hydrated Electrode Surfaces. *J. Chem. Phys.* **2012**, *138*, 184702.
(28) Limmer, D. T.; Willard, A. P.; Madden, P. A.; Chandler, D. Water Exchange at a Hydrated Platinum Electrode is Rare and Collective. *J. Phys. Chem. C* **2015**, *119*, 24016−24024.
(29) Limmer, D. T.; Willard, A. P. Nanoscale Heterogeneity at the Aqueous Electrolyte−Electrode Interface. *Chem. Phys. Lett.* **2015**, *620*, 144−150.
(30) Luzar, A.; Chandler, D. Hydrogen-Bond Kinetics in Liquid Water. *Nature* **1996**, *379*, 55−57.
(31) Luzar, A.; Chandler, D. Effect of Environment on Hydrogen Bond Dynamics in Liquid Water. *Phys. Rev. Lett.* **1996**, *76*, 928.
(32) Luzar, A. Resolving the Hydrogen Bond Dynamics Conundrum. *J. Chem. Phys.* **2000**, *113*, 10663.
(33) Starr, F. W.; Nielsen, J. K.; Stanley, H. E. Fast and Slow Dynamics of Hydrogen Bonds in Liquid Water. *Phys. Rev. Lett.* **1999**, *82*, 2294−2297.
(34) Eaves, J. D.; Loparo, J. J.; Fecko, C. J.; Roberts, S. T.; Tokmakoff, A.; Geissler, P. L. Hydrogen Bonds in Liquid Water Are Broken Only Fleetingly. *Proc. Natl. Acad. Sci. U. S. A.* **2005**, *102*, 13019−13022.
(35) Guàrdia, E.; Laria, D.; Martí, J. Hydrogen Bond Structure and Dynamics in Aqueous Electrolytes at Ambient and Supercritical Conditions. *J. Phys. Chem. B* **2006**, *110*, 6332−6338.
(36) Sciortino, F.; Poole, P. H.; Stanley, H. E.; Havlin, S. Lifetime of the Bond Network and Gel-Like Anomalies in Supercooled Water. *Phys. Rev. Lett.* **1990**, *64*, 1686−1689.
(37) Chandra, A. Effects of Ion Atmosphere on Hydrogen-Bond Dynamics in Aqueous Electrolyte Solutions. *Phys. Rev. Lett.* **2000**, *85*, 768−771.
(38) Kropman, M. F.; Bakker, H. J. Dynamics of Water Molecules in Aqueous Solvation Shells. *Science* **2001**, *291*, 2118−2120.
(39) Galamba, N. Water Tetrahedrons, Hydrogen-Bond Dynamics, and the Orientational Mobility of Water around Hydrophobic Solutes. *J. Phys. Chem. B* **2014**, *118*, 4169−4176.
(40) Rosenfeld, D. E.; Schmuttenmaer, C. A. Dynamics of the Water Hydrogen Bond Network at Ionic, Nonionic, and Hydrophobic Interfaces in Nanopores and Reverse Micelles. *J. Phys. Chem. B* **2011**, *115*, 1021−1031.
(41) Jana, M.; Bandyopadhyay, S. Kinetics of Hydrogen Bonds in Aqueous Solutions of Cyclodextrin and Its Methyl-Substituted Forms. *J. Chem. Phys.* **2011**, *134*, 025103.
(42) Xu, H.; Berne, B. J. Hydrogen-Bond Kinetics in the Solvation Shell of a Polypeptide. *J. Phys. Chem. B* **2001**, *105*, 11929−11932.
(43) Stirnemann, G.; Rossky, P. J.; Hynes, J. T.; Laage, D. Water Reorientation, Hydrogen-Bond Dynamics, and 2D-IR Spectroscopy Next to an Extended Hydrophobic Surface. *Faraday Discuss.* **2010**, *146*, 263−281.

DOI: 10.1021/acs.jpcc.6b07504
J. Phys. Chem. C 2016, 120, 27276−27284

(44) Hanasaki, I.; Nakatani, A. Hydrogen Bond Dynamics and Microscopic Structure of Confined Water inside Carbon Nanotubes. *J. Chem. Phys.* **2006**, *124*, 174714.
(45) Han, S.; Kumar, P.; Stanley, H. E. Hydrogen-Bond Dynamics of Water in a Quasi-Two-Dimensional Hydrophobic Nanopore Slit. *Phys. Rev. E* **2009**, *79*, 041202.
(46) Paul, S.; Chandra, A. Hydrogen-Bond Dynamics at Vapour−Water and Metal−Water Interfaces. *Chem. Phys. Lett.* **2004**, *386*, 218−224.
(47) Liu, P.; Harder, E.; Berne, B. J. Hydrogen-Bond Dynamics in the Air−Water Interface. *J. Phys. Chem. B* **2005**, *109*, 2949−2955.
(48) Ni, Y.; Gruenbaum, S. M.; Skinner, J. L. Slow Hydrogen-Bond Switching Dynamics at the Water Surface Revealed by Theoretical Two-Dimensional Sum-Frequency Spectroscopy. *Proc. Natl. Acad. Sci. U. S. A.* **2013**, *110*, 1992−1998.
(49) Siepmann, J. I.; Sprik, M. Influence of Surface Topology and Electrostatic Potential on Water/Electrode Systems. *J. Chem. Phys.* **1995**, *102*, 511−524.
(50) Martí, J.; Padró, J. A.; Guàrdia, E. Molecular Dynamics Calculation of the Infrared Spectra in Liquid H_2O−D_2O Mixtures. *J. Mol. Liq.* **1994**, *62*, 17−31.
(51) Toukan, K.; Rahman, A. Molecular-Dynamics Study of Atomic Motions in Water. *Phys. Rev. B: Condens. Matter Mater. Phys.* **1985**, *31*, 2643−2648.
(52) Chen, S.-H.; Toukan, K.; Loong, C.-K.; Price, D. L.; Teixeira, J. Hydrogen-Bond Spectroscopy of Water by Neutron Scattering. *Phys. Rev. Lett.* **1984**, *53*, 1360−1363.
(53) Yeh, I.-C.; Berkowitz, M. L. Ewald Summation for Systems with Slab Geometry. *J. Chem. Phys.* **1999**, *111*, 3155−3162.
(54) Wang, Z.; Yang, Y.; Olmsted, D. L.; Asta, M.; Laird, B. B. Evaluation of the Constant Potential Method in Simulating Electric Double-Layer Capacitors. *J. Chem. Phys.* **2014**, *141*, 184102.
(55) Kawata, M.; Mikami, M. Rapid Calculation of Two-Dimensional Ewald Summation. *Chem. Phys. Lett.* **2001**, *340*, 157−164.
(56) Gingrich, T. R.; Wilson, M. On the Ewald Summation of Gaussian Charges for the Simulation of Metallic Surfaces. *Chem. Phys. Lett.* **2010**, *500*, 178−183.
(57) Nosé, S. Unified Formulation of the Constant Temperature Molecular-Dynamics Methods. *J. Chem. Phys.* **1984**, *81*, 511−519.
(58) Hoover, W. G. Canonical Dynamics: Equilibrium Phase-Space Distributions. *Phys. Rev. A: At., Mol., Opt. Phys.* **1985**, *31*, 1695−1697.
(59) Laage, D.; Hynes, J. T. On the Molecular Mechanism of Water Reorientation. *J. Phys. Chem. B* **2008**, *112*, 14230−14242.
(60) Laage, D.; Stirnemann, G.; Sterpone, F.; Rey, R.; Hynes, J. T. Reorientation and Allied Dynamics in Water and Aqueous Solutions. *Annu. Rev. Phys. Chem.* **2011**, *62*, 395−416.
(61) Martí, J.; Guàrdia, E.; Padró, J. A. Dielectric Properties and Infrared Spectra of Liquid Water: Influence of the Dynamic Cross Correlations. *J. Chem. Phys.* **1994**, *101*, 10883−10891.
(62) For a comprehensive description of recent developments on surface sensitive experimental techniques see, for example, Zaera, F. *Chem. Rev.* **2012**, *112*, 2920−2986.
(63) Iwasita, T.; Xia, X. Adsorption of Water at Pt(111) Electrode in $HClO_4$ Solutions. The Potential of Zero Charge. *J. Electroanal. Chem.* **1996**, *411*, 95−102.
(64) Futamata, M.; Luo, L.; Nishihara, C. ATR-SEIR Study of Anions and Water Adsorbed on Platinum Electrode. *Surf. Sci.* **2005**, *590*, 196−211.
(65) Osawa, M.; Tsushima, M.; Mogami, H.; Samjeské, G.; Yamakata, A. Structure of Water at the Electrified Platinum−Water Interface: A Study by Surface-Enhanced Infrared Absorption Spectroscopy. *J. Phys. Chem. C* **2008**, *112*, 4248−4256.
(66) Ataka, K.-i.; Yotsuyanagi, T.; Osawa, M. Potential-Dependent Reorientation of Water Molecules at an Electrode/Electrolyte Interface Studied by Surface-Enhanced Infrared Absorption Spectroscopy. *J. Phys. Chem.* **1996**, *100*, 10664−10672.
(67) Ataka, K.-i.; Osawa, M. In-situ Infrared Study of Water−Sulfate Coadsorption on Gold(111) in Sulfuric Acid Solutions. *Langmuir* **1998**, *14*, 951−959.
(68) Hirota, L.; Song, M.-B.; Ito, M. In-Situ Infrared Spectroscopy of Water and Electrolytes Adsorbed on a Pt(111) Electrode Surface in Acid Solution. Structural Changes of Adsorbed Water Molecules upon an Electrode Potential. *Chem. Phys. Lett.* **1996**, *250*, 335−341.
(69) Xu, H.; Stern, H. A.; Berne, B. J. Can Water Polarizability Be Ignored in Hydrogen Bond Kinetics? *J. Phys. Chem. B* **2002**, *106*, 2054−2060.
(70) Perera, P. N.; Fega, K. R.; Lawrence, C.; Sundstrom, E. J.; Tomlinson-Phillips, J.; Ben-Amotz, D. Observation of Water Dangling OH Bonds around Dissolved Nonpolar Groups. *Proc. Natl. Acad. Sci. U. S. A.* **2009**, *106*, 12230−12234.
(71) Shen, Y. R.; Ostroverkhov, V. Sum-Frequency Vibrational Spectroscopy on Water Interfaces: Polar Orientation of Water Molecules at Interfaces. *Chem. Rev.* **2006**, *106*, 1140.
(72) Wang, Y.; Huang, X.; Shepler, B. C.; Braams, B. J.; Bowman, J. M. Flexible, Ab Initio Potential, and Dipole Moment Surfaces of Water. I. Tests and Applications for Clusters up to 22-mer. *J. Chem. Phys.* **2011**, *134*, 94509.
(73) Wang, Y.; Babin, V.; Bowman, J. M.; Paesani, F. The Water Hexamer-Cage, Prism or Both: Full Dimensional Quantum Simulations Say Both. *J. Am. Chem. Soc.* **2012**, *134*, 11116.
(74) Babin, V.; Leforestier, C.; Paesani, F. Development of a "First Principles" Water Potential with Flexible Monomers: Dimer Potential Energy Surface, VRT Spectrum, and Second Virial Coefficient. *J. Chem. Theory Comput.* **2013**, *9*, 5395−5403.
(75) Babin, V.; Medders, G. R.; Paesani, F. Development of a "First Principles" Water Potential with Flexible Monomers. II. Trimer Potential Energy Surface. *J. Chem. Theory Comput.* **2014**, *10*, 1599−1607.
(76) Babin, V.; Medders, G. R.; Paesani, F. Development of a "First-Principles" Water Potential with Flexible Monomers. III. Liquid Phase Properties. *J. Chem. Theory Comput.* **2014**, *10*, 2906−2910.
(77) Cisneros, G. A.; Wikfeldt, J. T.; Ojamäe, L.; Lu, J.; Xu, Y.; Torabifard, H.; Bartók, A.; Csányi, G.; Molinero, V.; Paesani, F. Modeling Molecular Interactions in Water: From Pairwise to Many-Body Potential Energy Functions. *Chem. Rev.* **2016**, *116*, 7501−7528.
(78) Ikeshoji, T.; Otani, M.; Hamada, I.; Okamoto, Y. Reversible Redox Reaction and Water Configuration on a Positively Charged Platinum Surface: First Principles Molecular Dynamics Simulation. *Phys. Chem. Chem. Phys.* **2011**, *13*, 20223−20227.
(79) Rossmeisl, J.; Nørskov, J. K.; Taylor, C. D.; Janik, M. J.; Neurock, M. Calculated Phase Diagrams for the Electrochemical Oxidation and Reduction of Water over Pt(111). *J. Phys. Chem. B* **2006**, *110*, 21833−21839.

DOI: 10.1021/acs.jpcc.6b07504
J. Phys. Chem. C 2016, 120, 27276−27284